

## Characterising the tidal stream power resource around France using a high-resolution harmonic database

Guillou, Nicolas; Neill, Simon; Robins, Peter

### Renewable Energy

Published: 01/08/2018

Peer reviewed version

[Cyswllt i'r cyhoeddiad / Link to publication](#)

*Dyfyniad o'r fersiwn a gyhoeddwyd / Citation for published version (APA):*

Guillou, N., Neill, S., & Robins, P. (2018). Characterising the tidal stream power resource around France using a high-resolution harmonic database. *Renewable Energy*, 123, 706-718.

#### Hawliau Cyffredinol / General rights

Copyright and moral rights for the publications made accessible in the public portal are retained by the authors and/or other copyright owners and it is a condition of accessing publications that users recognise and abide by the legal requirements associated with these rights.

- Users may download and print one copy of any publication from the public portal for the purpose of private study or research.
- You may not further distribute the material or use it for any profit-making activity or commercial gain
- You may freely distribute the URL identifying the publication in the public portal ?

#### Take down policy

If you believe that this document breaches copyright please contact us providing details, and we will remove access to the work immediately and investigate your claim.

# Characterising the tidal stream power resource around France using a high-resolution harmonic database

Nicolas Guillou<sup>a,\*</sup>, Simon P. Neill<sup>b</sup>, Peter E. Robins<sup>b</sup>

<sup>a</sup>*Laboratoire de Génie Côtier et Environnement (LGCE), Cerema, Direction Eau Mer et Fleuves, ER, 155 rue Pierre Bouguer, Technopôle Brest-Iroise, BP 5, 29280, Plouzané, France*

<sup>b</sup>*School of Ocean Sciences, Bangor University, LL59 5AB, United-Kingdom*

---

## Abstract

Although tidal stream energy is highly predictable, the distribution of the resource varies over small spatial scales and over tidal-to-decadal time scales, requiring detailed models and accurate analysis techniques. The present study investigates the spatial and temporal variability of the tidal stream energy resource around France, using a tidal current harmonic database. The 250 m resolution tidal database covers western Brittany and the western English Channel, two regions that have strong potential for tidal array development. As well as generating a refined resource assessment for the region, a series of simplified parameters are considered to assess resource variability, both spatially and temporally. Particular attention is dedicated to variability over spring-neap time scales (resulting from  $M_2$  and  $S_2$  compound tides) and current asymmetry (governed by  $M_2$  and  $M_4$  velocities). A clear contrast in the nature of the resource is found between sites located off the Cotentin Peninsula, which exhibit low spring-neap variability and

---

\*Corresponding author

*Email address:* nicolas.guillou@cerema.fr (Nicolas Guillou)

tidal asymmetry, leading to a more continuous and therefore attractive energy conversion, and sites in western Brittany, with greater variabilities over semi-diurnal and fortnightly time scales.

*Keywords:* spring-neap tidal variability, tidal current asymmetry, horizontal-axis turbines, Fromveur Strait, Paimpol-Bréhat, Alderney Race

---

## 1. Introduction

Technologies for tidal stream energy conversion are still in the early stages of development, although for many countries this sector has the potential to form a significant part of their future energy mix, contributing to a reduction in carbon dioxide emissions [1]. However, prior to commercial-scale deployment of tidal stream energy converters, a detailed characterisation of the ambient hydrodynamics is required to improve device design and determine optimum turbines' locations within a wider region of strong flows. Model-generated regional resource assessments are generally restricted to a reduced number of parameters, focusing primarily on the amplitudes of mean and peak tide-generated velocity and associated stream power [2, 3, 4, 5]. Whereas such resource assessments provide an initial characterisation for site selection based on the spatial distribution of resource hotspots, it is then necessary to characterise the temporal variability of the resource over semi-diurnal-to-decadal timescales.

Following this objective, advanced resource assessments have been conducted to characterise spatial and temporal variability of the resource, using tidal analysis to derive the major tidal current harmonic components from model simulations [6, 7, 8]. These large-scale investigations, mainly focusing

20 on the northwest European shelf seas, have provided detailed insights into  
21 tidal hydrodynamics that are particularly useful for potential device devel-  
22 opers; for example, by exhibiting the spring-neap tidal variabilities of the  
23 resource, the expected tidal asymmetry of flow and rectilinear misalignment  
24 [7], or the phase diversity between discrete potential tidal stream energy sites  
25 [8].

26 These studies [6, 7, 8] derived a tidal current harmonic database in order  
27 to evaluate the variability of the tidal stream energy resource beyond mean  
28 tidal conditions. The phase relationship between the principal semi-diurnal  
29  $M_2$  tidal current and its quarter-diurnal harmonic  $M_4$  may thus be calculated  
30 to characterise asymmetries in energy extraction over tidal time scales [9].  
31 Sites identified with lower spring-neap tidal variability, which is desirable  
32 for a more consistent tidal energy yield throughout the lunar cycle, can be  
33 identified by computing the ratio between current amplitudes of principal  
34 lunar  $M_2$  and solar  $S_2$  semi-diurnal harmonic constituents [7]. Tidal analysis  
35 can also expose regions of diurnal inequalities where consecutive tidal cycles  
36 are of unequal magnitude, and regions of lunar inequalities where consecutive  
37 spring-neap cycles vary significantly. Over longer time scales, this approach  
38 could evaluate inter-annual (or longer) variabilities in the resource, although  
39 this has not yet been investigated in the literature.

40 Tidal ellipses can furthermore be generated in order to determine the ori-  
41 entation of the flow as either rectilinear or more rotary in character [10, 11,  
42 12]. This approach can quantify the expected reduction in power due to rec-  
43 tilinear misalignment, helping developers optimise device design (e.g. fixed  
44 orientation, yawing, or floating-platform turbines). Making use of established

45 tidal current harmonic databases, rather than developing new models, has  
46 the additional advantage of increased spatial definition liable to incorporate  
47 local solutions between  $1/30$  and  $1/60^\circ$  in coastal areas [13].

48 Considering these aspects of resource variability, the present study inves-  
49 tigates the benefits associated with generating a high-resolution tidal current  
50 harmonic database for tidal stream resource assessments. Our study focuses  
51 on the waters around France, where the strongest tidal currents are located  
52 off western Brittany and in the English Channel (Fig. 1). This region hosts  
53 two full-scale test sites for horizontal-axis, bottom-mounted, turbines: (1)  
54 the OpenHydro demonstration farm off Paimpol-Brehat, and (2) the Sabella  
55 device in the Fromveur Strait between the isle of Ushant and the Molène  
56 archipelago (Figs. 1 and 2). In the western English Channel, this region cov-  
57 ers also the Alderney Race (“Raz Blanchard”), where a tidal farm of  $7 \times 2$   
58 MW horizontal-axis turbines is planned as part of the “Normandie Hydro”  
59 project (Fig. 2). This regional analysis will finally benefit from an exten-  
60 sive comparison with several local resource assessments in these tidal stream  
61 energy sites [14, 15, 16, 17, 18].

62 This investigation uses a tidal harmonic database of elevation and depth-  
63 averaged current components, covering western Brittany and the English  
64 Channel, at a consistent spatial resolution of 250 m (Section 2.1). When  
65 compared with regional investigations conducted at kilometric spatial reso-  
66 lutions, the 250 m resolution database used here has the potential to resolve  
67 the tidal hydrodynamics in narrow channels and in the vicinity of head-  
68 lands, both locations accounting for a high proportion of the potential tidal  
69 stream energy resource [8]. For each harmonic constituent, tidal current el-

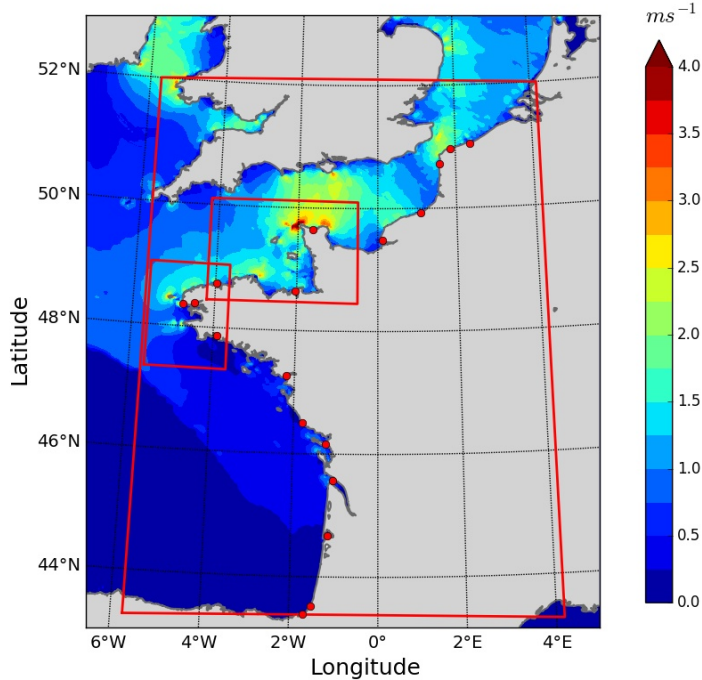


Figure 1: Maximum depth-averaged tidal current speeds during a year, recomposed from 10 primary harmonic constituents ( $M_2$ ,  $S_2$ ,  $N_2$ ,  $K_2$ ,  $K_1$ ,  $O_1$ ,  $P_1$ ,  $Q_1$ ,  $M_4$  and  $MS_4$ ), in north-west European shelf seas around France. Red lines delineate (1) computational domains over the English Channel and the Bay of Biscay and (2) high-resolution embedded domains off western Brittany and in the western English Channel. The positions of tide gauges used for the evaluation of elevation harmonic components are shown as red filled circles.

70 lipse parameters are derived from amplitudes and phases of eastward and  
 71 northward components (Section 2.2). We also characterise variabilities in  
 72 tidal stream power at quarter-diurnal and spring-neap time scales (Section  
 73 2.3). After an evaluation of the harmonic database based on a compari-  
 74 son between predicted and observed tidal currents (Section 3.1), the criteria  
 75 adopted by Robins et al. [7], which considers peak current speeds in excess

76 of  $2.0 \text{ m s}^{-1}$  in mean spring conditions and water depths over 25 m, is applied  
 77 to identify suitable locations for the deployment of turbines in marine areas  
 78 around France (Section 3.2). Particular attention is given to spring-neap  
 79 tidal variability and asymmetry in power extraction (Sections 3.3 and 3.4).  
 80 With respect to previous regional studies, additional investigations are finally  
 81 conducted on the orientation and ellipticity of tidal currents at potential tidal  
 82 stream energy sites.

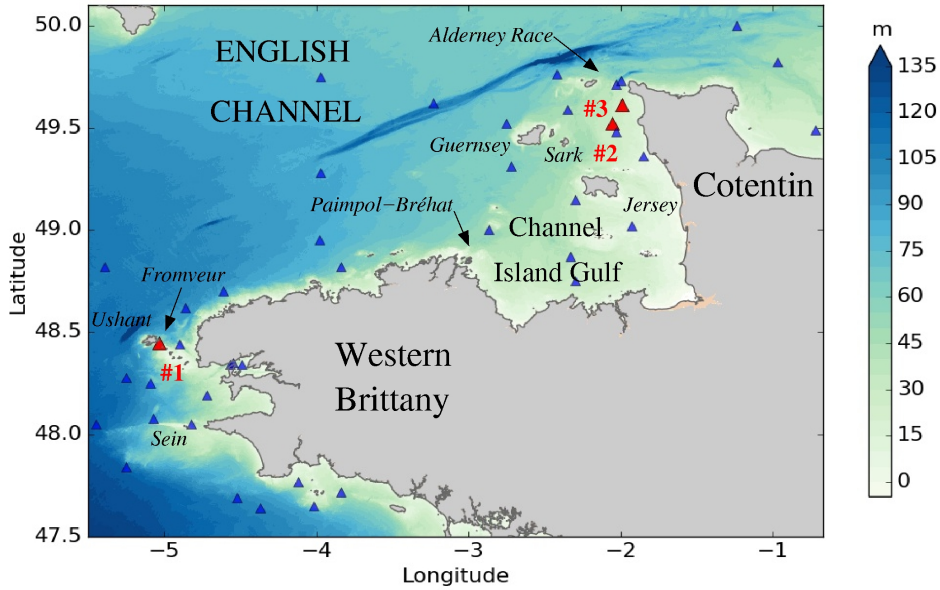


Figure 2: Bathymetry of western Brittany and the western English Channel (with respect to the lowest astronomical tide), with the locations of current meters in triangles. Blue triangles show the position of measurement points used for the assessment of MARS predictions. Red triangles (points #1, #2 and #3) correspond to locations selected, in the vicinity of major French tidal stream energy sites, for detailed evaluation of the current harmonic database.

## 83 **2. Materials and methods**

### 84 *2.1. Tidal harmonic database*

85 The tidal harmonic database considered here has been developed from nu-  
86 merical simulations with the circulation model MARS [19] applied to north-  
87 western Europe [20]. A depth-averaged version of the numerical model cov-  
88 ers three nested computational domains with spatial resolutions of: (1) 2 km  
89 across the northwest European shelf, (2) 700 m over the English Channel and  
90 the Bay of Biscay, and (3) 250 m in western Brittany and the western English  
91 Channel (Fig. 1). For the present investigation, we focus on outputs from  
92 the 250 m resolution coastal domains since, upon inspection of Fig. 1, these  
93 are the regions with the strongest resource. These nested models were driven  
94 by sea-surface elevations derived from tidal harmonic components developed  
95 by the French Navy SHOM (“Service Hydrographique et Océanographique  
96 de la Marine”) [21], and surges predicted by the large-scale models at 2 km  
97 and 700 m spatial resolutions. Numerical simulations include atmospheric  
98 forcings from the meteorological models ARPEGE and AROME of Météo-  
99 France [22, 23], with spatial and temporal resolutions of 0.5 and 0.025° and  
100 6 and 1 hours, respectively.

101 Coastal predictions, at 15 min time intervals, were analysed with the Tidal  
102 Toolbox software provided by LEGOS [24], to compute the amplitude and  
103 phase of elevation and current harmonic components. These results were  
104 available on a staggered Arakawa C-grid. Bi-linear spatial interpolations  
105 were implemented to obtain all components at the center of the grid cells. As  
106 recommended by Pineau-Guillou [20], results close to offshore sea boundaries  
107 (in a band of 10% of the computational domain) were not considered in the



108 present investigation.

109 *2.2. Analysis of tidal currents*

110 In the tidal database, the current of a given harmonic constituent is rep-  
111 resented as eastward and northward components

$$\begin{cases} east & = U \cos(\omega t - \phi_u) , \\ north & = V \cos(\omega t - \phi_v) \end{cases} \quad (1)$$

112 where  $(U, V)$  and  $(\phi_u, \phi_v)$  are the associated amplitudes (m) and phases  
113 (degrees relative to Greenwich), respectively (Fig. 3),  $t$  is time (s) and  $\omega =$   
114  $2\pi/T$  is the angular frequency of the harmonic component with  $T$  (s) the  
115 tidal period. However, specific computational methods are required to obtain  
116 current ellipse parameters, which characterise the magnitude, orientation

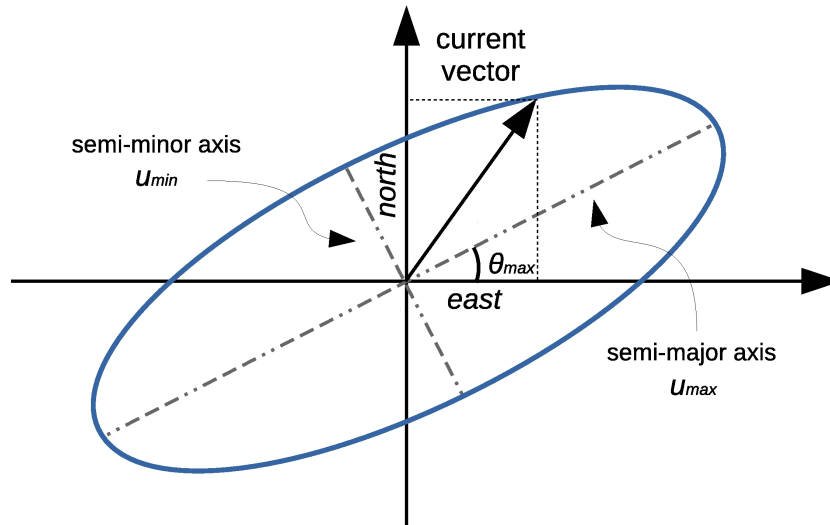


Figure 3: Schematic representation of a tidal current ellipse for a single harmonic current component with associated parameters.

117 and variation of associated tidal stream currents and, in turn, power. This  
118 mathematical problem may be illustrated with the approach of the ellipse  
119 semi-major axis (Fig. 3). Indeed, the amplitude of this axis, which accounts  
120 for the maximum current speed over the tidal period, cannot be directly  
121 computed from  $U$  and  $V$ , mainly as associated components are characterised  
122 by different phases  $\phi_u$  and  $\phi_v$ . Two methods are available to compute tidal  
123 current ellipse parameters: the first deals with trigonometric formulations,  
124 the second relies on a less intuitive parameterisation in terms of polar vectors  
125 [11]. The first method is applied here. As further details about the associated  
126 formulations are available in Pugh [11] and elsewhere, this section resumes  
127 the mathematical expression used in the present study. The maximum and  
128 minimum values of the current speed, also defined as the semi-major and  
129 semi-minor axes of the ellipse, are thus obtained from the following two  
130 equations:

$$u_{max} = \left( \frac{U^2 + V^2 + \alpha^2}{2} \right)^{1/2}, \quad (2)$$

$$u_{min} = \left( \frac{U^2 + V^2 - \alpha^2}{2} \right)^{1/2} \quad (3)$$

131 with  $\alpha^2 = [U^4 + V^4 + 2U^2V^2 \cos(2(\phi_u - \phi_v))]$ <sup>1/2</sup>. The rectilinear/circular  
132 nature of the tidal current ellipse is determined from the angle:

$$\beta = \arctan \left( \frac{u_{min}}{u_{max}} \right), \quad (4)$$

133 which accounts for the ellipticity of the current hodograph<sup>1</sup>. Low values of  
134  $\beta$  close to  $0^\circ$  indicate rectilinear currents, while values close to  $45^\circ$  imply

---

<sup>1</sup>A diagram that provides a vectorial visual representation of the movement of a body or a fluid.

135 almost circular evolutions. The tidal current vector reaches the maximum  
 136 amplitude  $u_{max}$  when  $\omega t = \text{phase} = \phi_u - \delta \pm 180^\circ$ , with  $\delta$  an angle obtained  
 137 from the following relationship:

$$\delta = \frac{1}{2} \arctan \left( \frac{V^2 \sin(2(\phi_u - \phi_v))}{U^2 + V^2 \cos(2(\phi_u - \phi_v))} \right). \quad (5)$$

138 The direction of the maximum current speed is finally given by

$$\theta_{max} = \arctan \left( \frac{V \cos(\phi_u - \phi_v - \delta)}{U \cos(\delta)} \right). \quad (6)$$

139 In cases where different harmonic components are considered, this method  
 140 cannot be applied, and requires the extraction of the maximum value of the  
 141 recomposed time series of the tidal current over a duration compatible with  
 142 the tidal periods integrated.

### 143 *2.3. Tidal energy resource metrics*

144 Following the study of Robins et al. [7] at the scale of the northwest  
 145 European shelf seas, a series of parameters are considered here to characterise  
 146 spatial and temporal variabilities of tidal currents and associated stream  
 147 power in coastal areas around France. Attention is primarily given to the  
 148 variability of tidal currents at fortnightly and semi-diurnal time scales, setting  
 149 aside analysis on diurnal inequalities, which appear to be of reduced influence  
 150 in western Brittany and the western English Channel [7] (Section 3.2). The  
 151 tidal current harmonic components analysed describe the spring-neap tidal  
 152 variability of the resource and the asymmetry of tidal currents between the  
 153 flood and ebb phases of the tidal cycle.

154 At potential tidal stream energy sites, minimal differences between spring  
 155 and neap currents are considered desirable, as this leads to a more consistent

156 energy yield over the fortnightly spring-neap period. Tidal kinetic energy  
 157 converters, designed to operate over a restricted range of velocities [25], do  
 158 not appear to be adapted to hydrodynamic environments with high spring-  
 159 neap tidal variability. Following Robins et al. [7], this variability is here  
 160 characterised by the ratio  $R_{var}$  between the maximum amplitudes of the  
 161 principal lunar  $M_2$  and solar  $S_2$  depth-averaged velocities,  $u_{max}(M_2)$  and  
 162  $u_{max}(S_2)$ :

$$R_{var} = 1 - \frac{u_{max}(S_2)}{u_{max}(M_2)}. \quad (7)$$

163 Over the northwest European shelf seas, as the amplitude of  $S_2$  velocities  
 164 are always weaker than the principal  $M_2$  velocities,  $R_{var}$  varies between 0  
 165 and 1. Values of  $R_{var}$  close to unity account for reduced spring-neap tidal  
 166 variability, whilst values close to zero show noticeable differences between the  
 167 spring and neap tidal cycles. Particular attention is furthermore devoted to  
 168 the modifications of current directions between simple  $M_2$  components and  
 169 combined  $M_2$  and  $S_2$  harmonic constituents. Following Lewis et al. [26], this  
 170 influence is exhibited by characterising misalignment between the flood and  
 171 ebb current directions during mean spring conditions:

$$\theta_{var} = \arccos \left( \frac{-\vec{u}_{flood} \cdot \vec{u}_{ebb}}{|\vec{u}_{flood}| \cdot |\vec{u}_{ebb}|} \right) \quad (8)$$

172 where  $\vec{u}_{flood}$  and  $\vec{u}_{ebb}$  are the peak velocity vectors during flood and ebb  
 173 periods at the location considered during mean spring conditions resulting  
 174 from  $M_2$  and  $S_2$  harmonic components. Low values of  $\theta_{var}$  characterise a  
 175 reduced asymmetry in current direction, whereas higher values account for a  
 176 strong tidal current misalignment.

177 At the semi-diurnal time scale, current asymmetry is another key param-  
 178 eter which characterises the variability in power production between flood

179 and ebb. As inferred by Pingree and Griffiths [27] and Friedrichs and Aubrey  
180 [28], asymmetry in tidal currents may arise from the phase relationship be-  
181 tween the principal semi-diurnal  $M_2$  and its first quarter-diurnal  $M_4$  har-  
182 monic. Adopting the parameterisation described in Section 2.2, maximum  
183 asymmetry is thus obtained when peak velocities of harmonic current vec-  
184 tors appear at the same time, which results in the following relationship:  
185  $\gamma = 2\text{phase}(M_2) - \text{phase}(M_4) = 0^\circ$  or  $180^\circ$  in the range  $[0, 360^\circ]$ . Symmetry  
186 of tidal currents occurs when  $M_2$  and  $M_4$  constituents are out of phase with  
187  $\gamma = 90^\circ$  or  $270^\circ$ . As the ratio between semi- and quarter-diurnal tidal cur-  
188 rent amplitude directly exacerbates this asymmetry, a parameter based on  
189 Robins et al. [7], is adopted here relying on ellipse characteristics:

$$A_1 = \frac{u_{max}(M_4)}{u_{max}(M_2)} |\cos(\gamma)| . \quad (9)$$

190 High values of  $A_1$  in the range  $[0,1]$  account for significant tidal asymmetry,  
191 whilst low values indicate more symmetrical currents. In order to ascertain  
192 the reliability of this parameter, a comparison is performed with a more  
193 classical approach of tidal current asymmetry based on the ratio of peak  
194 tidal currents, resulting from  $M_2$  and  $M_4$  components, during flood and ebb:

$$A_2 = 1 - \frac{u_{peak,1}}{u_{peak,2}} \quad (10)$$

195 where  $u_{peak,2}$  is the maximum of the peak velocity between flood and ebb and  
196  $u_{peak,1}$  is the minimum peak velocity. This parameter, which varies between  
197 0 and 1, should therefore be consistent with  $A_1$ .

### 198 **3. Results and discussion**

#### 199 *3.1. Validation of the tidal harmonic database*

200 The harmonic database has been assessed by Pineau-Guillou [20] by com-  
201 paring recomposed tidal water elevations with observations at a series of 18  
202 harbours along the coasts of France (Fig. 1). The root mean square error  
203 (RMSE) between predictions and observations was calculated, on average, at  
204 around 20 cm, matching with the range of mean surges. Maximum RMSE of  
205 27 cm is obtained at Boulogne-sur-Mer in the Dover Strait (eastern English  
206 Channel). These evaluations have been extended by comparing predicted  
207 and observed harmonic components of surface elevations. The spatial dis-  
208 tribution of major elevation components  $M_2$  and  $S_2$ , at tide gauges, is thus  
209 approached with differences less than 5% for amplitude and  $8^\circ$  for phase.  
210 Further details about the evaluation of the elevation harmonic database are  
211 available in Pineau-Guillou [20].

212 Coastal current predictions of MARS, used to establish the harmonic  
213 database (Section 2.1), have been compared with observations compiled by  
214 the French Navy SHOM, measured during spring tide conditions, at a series  
215 of 37 locations over western Brittany and the western English Channel (Fig.  
216 2) [29]. In addition, the validation has been extended to include a series of  
217 three available ADCP deployments in two areas with strong potential for the  
218 exploitation of the tidal kinetic energy resource: the Fromveur Strait and  
219 the Alderney Race. These observations include (see Fig. 2 and Table 1):  
220 (1) long-term records conducted by SHOM in western Brittany (point #1),  
221 and (2) two short-term campaigns implemented by Bailly du Bois [30] in the  
222 western English Channel (points #2 and #3).

223 In relation to the availability of in-situ data, the validation in western  
224 Brittany was performed at 10 m above the seabed – this elevation corre-  
225 sponds to the operating height of proposed horizontal axis turbines in French  
226 tidal stream energy sites (Fig. 4). Following Guillou and Thiébot [17], the  
227 tidal currents at 10 m above the seabed were obtained from the recomposed  
228 depth-averaged currents by assuming a vertical logarithmic velocity profile  
229 with a bottom roughness parameter set to  $z_0 = 20$  mm. Whereas a Strickler  
230 law is adopted in the depth-averaged MARS model [29], this roughness value  
231 of  $z_0 = 20$  mm, adopted over bottom rock outcrops in the Fromveur Strait,  
232 provided the best estimates of current amplitude and direction at point #1  
233 [17]. Depth-averaged currents are recomposed from the 10 primary harmonic  
234 components:  $M_2$ ,  $S_2$ ,  $N_2$ ,  $K_2$ ,  $K_1$ ,  $O_1$ ,  $P_1$ ,  $Q_1$ ,  $M_4$  and  $MS_4$ . In spite of a ten-  
235 dency to overestimate spring current magnitudes, seemingly associated with  
236 different parameterisations of bottom friction, and exhibited by the positives  
237 values of the mean relative difference  $\text{DIFF}_{\text{rel}}$  (Tab. 2), the numerical results  
238 reproduce the variations of tidal velocity, in particular, the abrupt changes  
239 between south-west and north-east directions (Fig. 4).

240 The evaluation of depth-averaged current amplitude in the western En-  
241 glish Channel (Fig. 5) confirms the ability of the coastal harmonic database  
242 to characterise tidal velocities, with RMSE restricted to  $0.16 \text{ m s}^{-1}$ . Further,  
243 variation of current direction is estimated with an index of agreement RE [31]  
244 over 0.98 at both measurements points #2 and #3. Stronger differences, ob-  
245 tained at point #3, may be associated with tidal recirculations in the vicinity  
246 of surrounding headlands that are not fully resolved in the model.

247 Finally, additional investigations show that the recomposed maximum

248 depth-averaged velocities based on  $M_2$  and  $S_2$  components, i.e. the mean  
 249 spring peak currents (Fig. 6), are consistent with current maps established  
 250 by the SHOM and EDF R&D over western Brittany and the western English  
 251 Channel [32], identifying areas of strong velocity amplitudes with differences  
 252 restricted to  $0.2 \text{ m s}^{-1}$ .

Table 1: Details of ADCP deployments.

Measurement points	Coordinates		Water depths (m)	Periods of measurements
	Lon.	Lat.		
#1	$5.036^\circ \text{ W}$	$48.449^\circ \text{ N}$	53	19/03/1993 $\rightarrow$ 02/04/1993
#2	$2.055^\circ \text{ W}$	$49.522^\circ \text{ N}$	29	10/08/2003 $\rightarrow$ 12/08/2003
#3	$1.993^\circ \text{ W}$	$49.614^\circ \text{ N}$	25	09/08/2003 $\rightarrow$ 11/08/2003

Table 2: Statistical parameters for the evaluation of observed currents amplitude  $U$  and direction  $Dir$  at points #1, #2 and #3: the mean relative difference  $\text{DIFF}_{\text{rel}}$ , the root mean square error RMSE and the index of agreement RE [31].

Measurement points	$U$			$Dir$		
	$\text{DIFF}_{\text{rel}}$	RMSE	RE	$\text{DIFF}_{\text{rel}}$	RMSE	RE
#1	$0.18 \text{ m s}^{-1}$	$0.31 \text{ m s}^{-1}$	0.96	$-6.7^\circ$	$36.0^\circ$	0.96
#2	$0.06 \text{ m s}^{-1}$	$0.09 \text{ m s}^{-1}$	0.97	$2.1^\circ$	$19.3^\circ$	0.99
#3	$0.10 \text{ m s}^{-1}$	$0.16 \text{ m s}^{-1}$	0.96	$-5.7^\circ$	$24.7^\circ$	0.98

### 253 3.2. Identification of potential tidal stream energy sites

254 In the majority of resource assessments around the United Kingdom  
 255 [7, 26, 33, 34], the identification of potential tidal stream energy sites is  
 256 mainly based on current speeds and water depths, neglecting further con-  
 257 strains associated with the practical, political, or environmental issues or



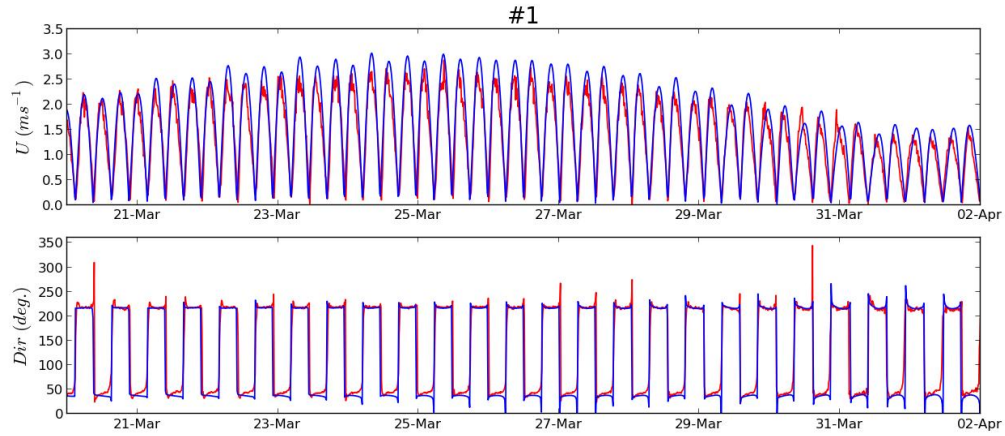


Figure 4: Recomposed (blue line) and observed (red line) time series of current amplitude and direction (anticlockwise convention from the East) 10 m above the seabed at point #1 in March-April 1993.

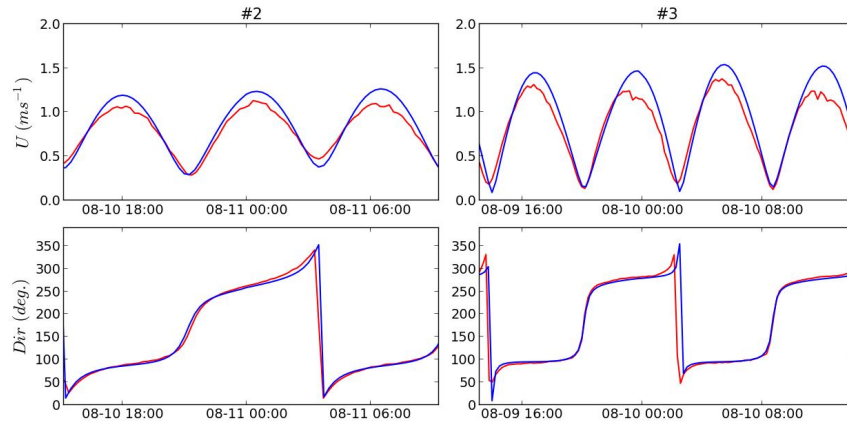


Figure 5: Recomposed (blue line) and observed (red line) time series of depth-averaged current amplitude and direction (anticlockwise convention from the East) at points #2 and #3 in August 2003.

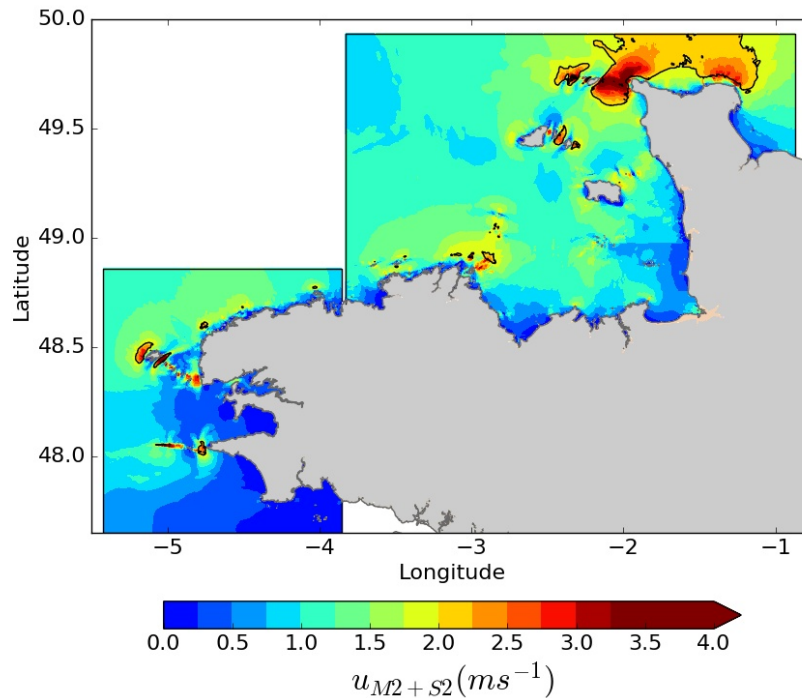


Figure 6: Maximum depth-averaged velocities from  $M_2$  and  $S_2$  harmonic components in western Brittany and the western English Channel. The black contours delineate potential tidal stream energy sites characterised by mean spring peak velocities over  $2 \text{ m s}^{-1}$  and water depths over 25 m.

258 marine activities. The present resource assessment is based on the criteria  
 259 adopted by Robins et al. [7] to identify potential locations for first- and  
 260 second-generation technologies of tidal stream energy converters, covering  
 261 both existing prototype devices in pre-commercial demonstration and at the  
 262 early stages of technology readiness [34]. This corresponds to areas with: (1)  
 263 peak current speeds in excess of  $2.0 \text{ m s}^{-1}$  in mean spring conditions, and (2)  
 264 a minimum water depth of 25 m. Further insights may be provided about  
 265 these limits from a rationale based on the output power formula of horizontal-

266 axis turbines  $P_{out} = (\rho C_p \pi D^2 u^3)/8$  with  $\rho$  the density of sea water ( $\text{kg m}^{-3}$ ),  
 267  $C_p$  the power coefficient,  $D$  the blade diameter (m) and  $u$  the tidal current  
 268 speed ( $\text{m s}^{-1}$ ).

269 Taking into account a range of device power coefficients [25], it is thus  
 270 necessary to have a peak current speed of at least  $2.0 \text{ m s}^{-1}$  in combination  
 271 with a minimum turbine diameter of 20 m to attain a power output of 0.5  
 272 MW, the lowest threshold of most horizontal-axis turbines currently tested  
 273 and implemented at potential tidal stream energy sites (Fig. 7). The min-  
 274 imum current speed is  $2.5 \text{ m s}^{-1}$  to attain a power output of 1 MW with  
 275 the same device characteristics. In order to ensure a constant immersion  
 276 of devices and sufficient navigational clearance, a minimum water depth of  
 277 around 25 m is required for this type of tidal stream power extraction.

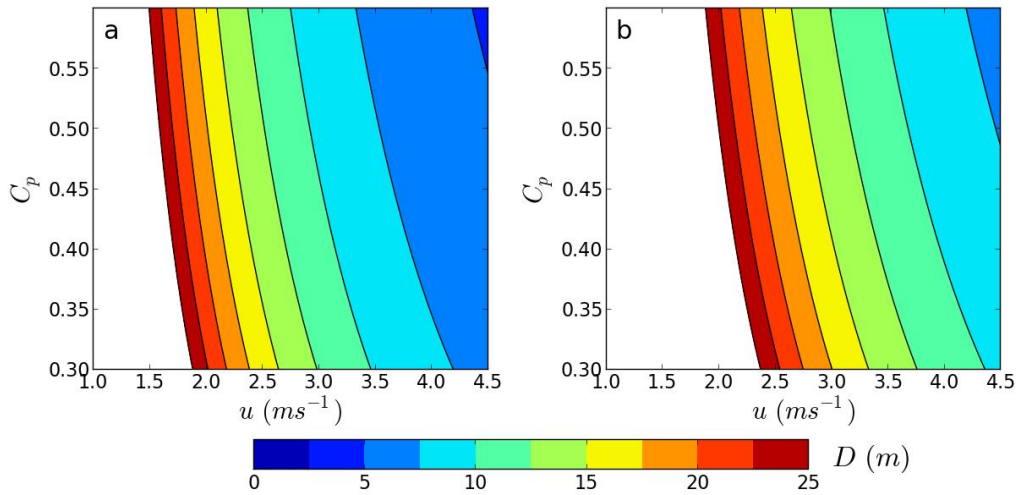


Figure 7: Minimum turbine diameter required to achieve power outputs of (a) 0.5 and (b) 1 MW, with respect to power coefficient  $C_p$  and tidal current velocity  $u$ . Diameters over 25 m are not shown on the figure.

278 In the present study, the criteria adopted for site selection considers  
279 the mean spring peak velocities resulting from  $M_2$  and  $S_2$  harmonic cur-  
280 rent components in the high-resolution coastal database (Section 2.1), and  
281 the water depth extracted from the HOMONIM (“Historique, Observation,  
282 MOdélisation des Niveaux Marins”, SHOM, Météo-France) database [35, 36]  
283 which covers the areas of interest at a spatial resolution of 111 m.

284 Along the coasts of France, potential tidal stream energy sites are mainly  
285 identified in western Brittany and the western English Channel (Fig. 6).  
286 Whereas all sites are characterised by a mean kinetic power density that  
287 exceeds  $0.8 \text{ kW m}^{-2}$  during a mean spring tidal cycle, the western area of  
288 Alderney (Casquets), the Alderney Race and the Fromveur Strait are the  
289 three locations where this power density significantly exceeds  $2.5 \text{ kW m}^{-2}$   
290 – meeting the resource criteria adopted by the Carbon Trust [37] for the  
291 deployment of first-generation turbine devices (Fig. 8, Table 3). The refined  
292 calculation of kinetic power density over these regions appears consistent  
293 with predictions from high-resolution nested numerical models. These results  
294 show: (1) in the Fromveur Strait, zones of high energy formed in between  
295 the islands with peak power density in each zone ranging from  $4 \text{ kW m}^{-2}$  to  
296 over  $7 \text{ kW m}^{-2}$  [16, 17], and (2) in the Alderney Race, a concentration of  
297 tidal stream energy over  $10 \text{ kW m}^{-2}$  around the Cotentin Peninsula [15, 18].  
298 Areas identified off the Cotentin Peninsula and in the Alderney Race are  
299 particularly remarkable, accounting for a total surface of around  $1750 \text{ km}^2$  in  
300 the embedded coastal domain. The mean power density associated with this  
301 potential sea space is estimated at  $1.6 \text{ kW m}^{-2}$ , with minimum and maximum  
302 values of  $0.9$  and  $12.4 \text{ kW m}^{-2}$ , respectively. However, the total surface is

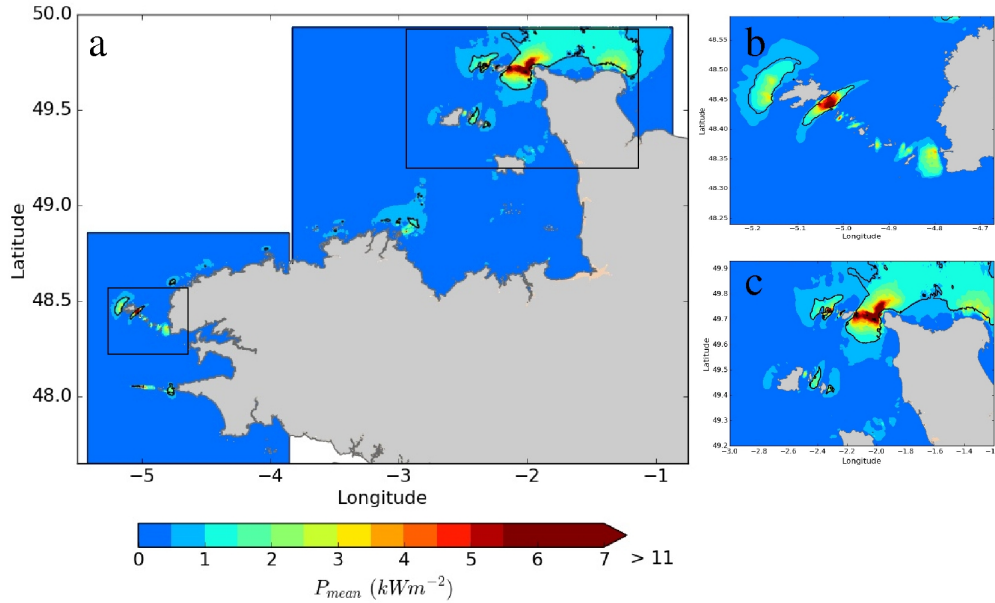


Figure 8: Mean kinetic power density distribution during a spring-neap tidal cycle ( $T=14.765$  days)) resulting from  $M_2$  and  $S_2$  components in (a) coastal domains, with magnified views in (b) the Fromveur Strait and (c) the Alderney Race. The black lines delineate potential tidal stream energy sites identified in Fig. 6.

303 markedly reduced by 80% to  $350 \text{ km}^2$  if a threshold of mean spring peak  
 304 velocity of  $2.5 \text{ m s}^{-1}$  is imposed. This difference highlights, in particular, the  
 305 increased sea space associated with the development of tidal stream turbine  
 306 technologies more suited to harnessing less energetic tidal streams. It should  
 307 finally be noted that the area located west of Alderney (Casquets) accounts  
 308 for a total surface of  $90 \text{ km}^2$ , with averaged power density during a mean  
 309 spring tidal cycle liable to exceed  $9 \text{ kW m}^{-2}$  (Table 3).

310 Outside of these significant areas, potential tidal stream energy sites oc-  
 311 cupy surfaces restricted to  $40 \text{ km}^2$  – predominantly in the vicinity of head-  
 312 lands and straits, confirming previous investigations conducted by Neill et

Table 3: Characteristics of major potential tidal stream energy sites associated with the averaged kinetic power distribution during a spring-neap tidal cycle resulting from  $M_2$  and  $S_2$  components (Fig. 8): total surface, mean power density  $P_{mean}$ , minimum and maximum values of the averaged power density  $P_{min}$  and  $P_{max}$  over the sea space of tidal stream energy sites.

Sites	Areal extent ( km <sup>2</sup> )	$P_{mean}$ ( kW m <sup>-2</sup> )	$P_{min}$ ( kW m <sup>-2</sup> )	$P_{max}$ ( kW m <sup>-2</sup> )
Raz of Sein	15	1.4	0.9	2.8
West of Ushant	40	1.4	0.8	3.2
Fromveur Strait	17	2.9	0.9	7.9
North-western Brittany	7	1.1	0.9	1.7
Paimpol-Bréhat	18	1.1	0.9	1.8
East of Sark	8	1.4	0.9	2.6
East of Guernsey (Big Roussel)	26	1.5	0.9	2.3
West of Alderney (Casquets)	90	1.5	0.9	9.9
Off Cotentin Peninsula	1753	1.6	0.9	12.4

313 al. [8]. Over these areas, the mean value of the associated power density is  
314 estimated between 1.1 and 1.5 kW m<sup>-2</sup> with peak values below 3.2 kW m<sup>-2</sup>  
315 (Table 3). These locations include the well-known French tidal stream energy  
316 sites in the Raz of Sein and off Paimpol-Bréhat, and also potential locations  
317 to the west of Ushant island and to the east of Guernsey (Big Roussel). In  
318 the Channel Islands Gulf, our resource assessment confirms conclusions from  
319 reports commissioned by the Carbon Trust [33, 38]. However, potential sites  
320 off the northwest coast of Guernsey and off the northeast coast of Jersey were  
321 not identified here. This is consistent with results obtained by Coles et al.  
322 [18] with a depth-averaged tidal circulation model covering these areas with  
323 a mesh resolution of 250 m. Other potential tidal stream energy sites with

324 surfaces areas less than  $8 \text{ km}^2$  are also identified along the northern coast of  
325 western Brittany and to the east of Sark. Over these two regions, the mean  
326 power density is estimated at  $1.1$  and  $1.4 \text{ kW m}^{-2}$ , respectively (Table 3).

327 We investigated the rectilinear/circular nature of tidal currents by focus-  
328 ing on the ellipticity associated with the principal lunar semi-diurnal compo-  
329 nent  $M_2$  (Fig. 9). In the English Channel, the spatial distribution of param-  
330 eter  $\beta$  (Eq. 4) appears consistent with the numerical investigation conducted  
331 by Fornerino and Le Provost [10], indicating strong gyrotory currents in the  
332 areas surrounding Guernsey and Jersey. However, with the exception of sites  
333 identified in the Raz of Sein and to the west of Alderney, the values of  $\beta$  for  
334  $M_2$  were less than  $5^\circ$  at potential tidal stream energy sites. This means that  
335 these sites contain near rectilinear  $M_2$  tidal currents, a key property required  
336 for the installation of horizontal-axis turbines with a fixed orientation.

337 Finally, the capacity factor of a series of horizontal-axis turbines varying  
338 in rated power is evaluated in order to provide potential developers further  
339 insights into device operating times (Fig. 10). Indeed, the capacity factor  
340 accounts for the fraction of the year the turbine generator is operating at  
341 rated power. Capacity factor was thus computed, defined as the averaged  
342 power produced over a year divided by the rated turbine power. This analysis  
343 relies on velocities recomposed from the 10 primary tidal harmonic compo-  
344 nents used to calculate Fig. 1. The power curves considered are based on the  
345 OpenHydro device [39], by assuming a cut-in speed of  $0.7 \text{ m s}^{-1}$  and rated  
346 speeds of  $1.7$ ,  $2.1$ ,  $2.5$  and  $2.7 \text{ m s}^{-1}$ , matching rated powers of  $0.5$ ,  $1.0$ ,  $1.5$   
347 and  $2.0 \text{ MW}$ , respectively. The capacity factor of  $0.5 \text{ MW}$  devices exceeds  
348  $40\%$  in most potential tidal stream energy sites, with maximum values over

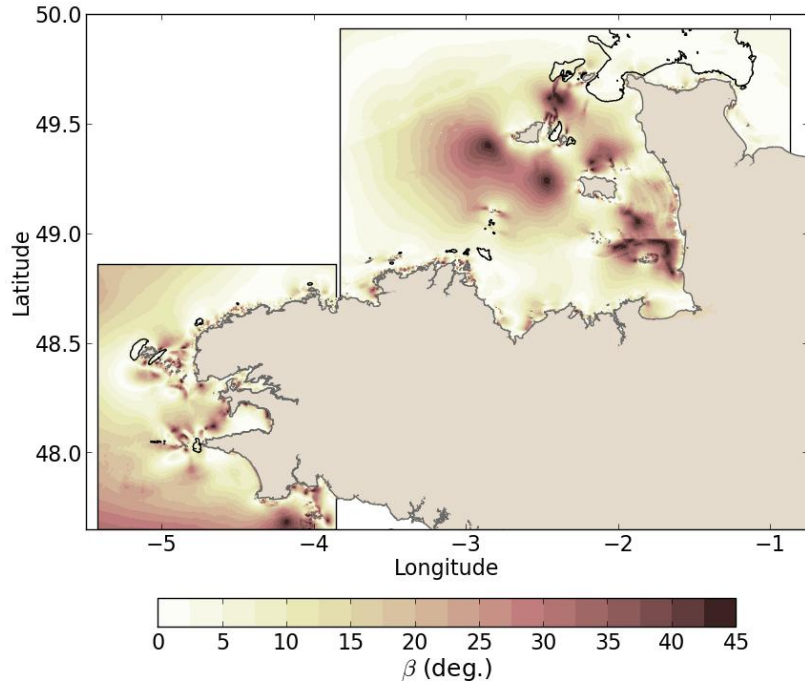


Figure 9: Spatial distribution of angle  $\beta$  (Eq. 4), characterising the ellipticity of  $M_2$  tidal currents in western Brittany and the western English Channel. The black lines delineate potential tidal stream energy sites identified in Fig. 6.

349 70% in the Fromveur Strait, the Alderney Race and west of Alderney in  
 350 relation to higher current speeds (Fig. 10-a). The capacity factor is natu-  
 351 rally reduced for higher rated powers with values restricted to 35% for 1.5  
 352 MW turbines in most potential locations, with exceptions in the three sites  
 353 previously identified (Fig. 10-c). However, the associated averaged power is  
 354 found to increase for high rated power. In the Alderney Race, the averaged  
 355 power produced over a year is thus restricted to 0.3 MW for 0.5 MW devices,  
 356 whereas it would exceed 1.1 MW for 2 MW turbines.



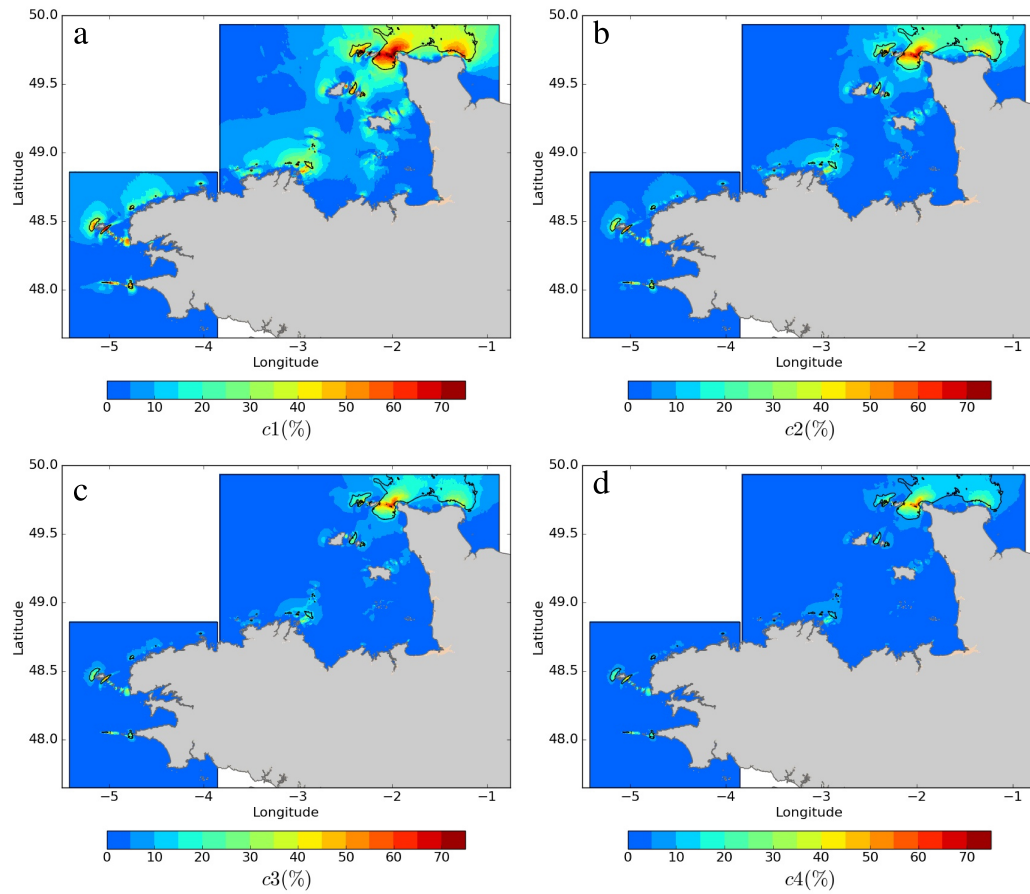


Figure 10: Annual capacity factor based on power curves with rated powers of (a) 0.5, (b) 1.0, (c) 1.5 and (d) 2.0 MW. The black lines delineate the potential tidal stream energy sites identified in Fig. 6.

### 357 3.3. Spring-neap variability

358 Confirming the investigation conducted by Robins et al. [7] over the  
359 north-west European shelf seas,  $R_{var}$  (Eq. 7) varies between 0.55 and 0.80  
360 in western Brittany and the western English Channel (Fig. 11). A clear  
361 gradient of the spring-neap tidal variability of currents is exhibited in the  
362 Channel Islands between a south-western area characterised by high vari-  
363 ability ( $R_{var} < 0.61$ ) and a north-eastern region with reduced variability  
364 ( $R_{var} > 0.67$ ). This difference is exhibited between the Alderney Race and  
365 the Fromveur Strait by retaining two locations with contrasting values of  
366  $R_{var} = 0.629$  in the Fromveur Strait (point p1) and  $R_{var} = 0.695$  in the  
367 Alderney Race (point p2).

368 Fig. 12 displays the extracted depth-averaged velocities resulting from  
369  $M_2$  and  $S_2$  harmonic components and the generated “technical” resource by  
370 applying the power curve of a 1.5 MW OpenHydro device and by neglecting  
371 turbine interactions and feedback between energy extraction and the hydro-  
372 dynamics. While the tidal velocity reaches slightly stronger magnitudes at  
373 the location considered in the Fromveur Strait ( $u_{max} = 3.41 \text{ m s}^{-1}$  at point  
374 p1 against  $3.36 \text{ m s}^{-1}$  at point p2), currents generate less power than at the  
375 point retained in the Alderney Race. The generated power over a mean  
376 spring-neap tidal cycle is thus estimated at 223 MWh at point p1 while it  
377 reaches 235 MWh at point p2. Whereas this difference accounts for about 5%  
378 of the total spring-neap generated power, with capacity factors estimated at  
379 42.1 and 44.2%, differences between sites increase significantly during neap  
380 tide conditions. Indeed, both locations show maximum spring tidal current  
381 velocities over the rated speed of the OpenHydro device, with differences in

382 generated power mainly attributed to neap conditions. During neap tides,  
 383 the maximum generated power is thus estimated at 0.63 MW at point p2,  
 384 while it is restricted to 0.43 MW at point p1 (Fig. 12).

385 Further investigations, conducted to calculate tidal current misalignment,  
 386 depict low values of the parameter  $\theta_{var}$  (Eq. 8); restricted to  $2^\circ$  between the  
 387 flood and ebb current directions of peak mean spring currents, in the majority  
 388 of potential tidal stream energy sites. Such misalignment direction lies below  
 389 the limit under which power reductions may be apparent for horizontal-fixed

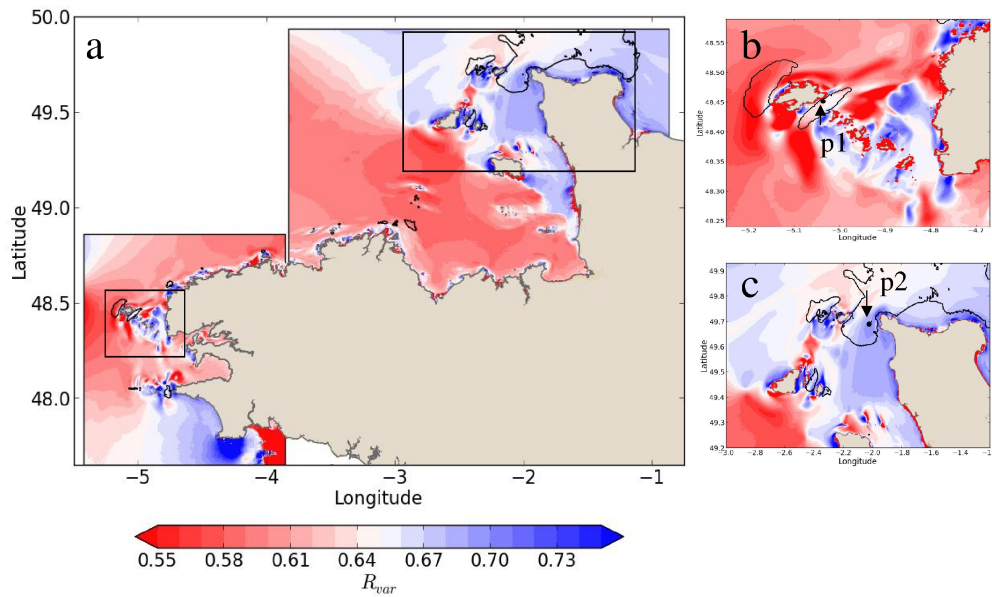


Figure 11: Spatial distribution of parameter  $R_{var}$ , characterising the variability of tidal current amplitude over a mean spring-neap cycle in (a) coastal domains, with magnified views in (b) the Fromveur Strait and (c) the Alderney Race. The black circles in (b) and (c) show the positions of points p1 and p2 used for the extraction of recomposed currents amplitude and direction (Fig. 12). The black lines delineate potential tidal stream energy sites identified in Fig. 6.

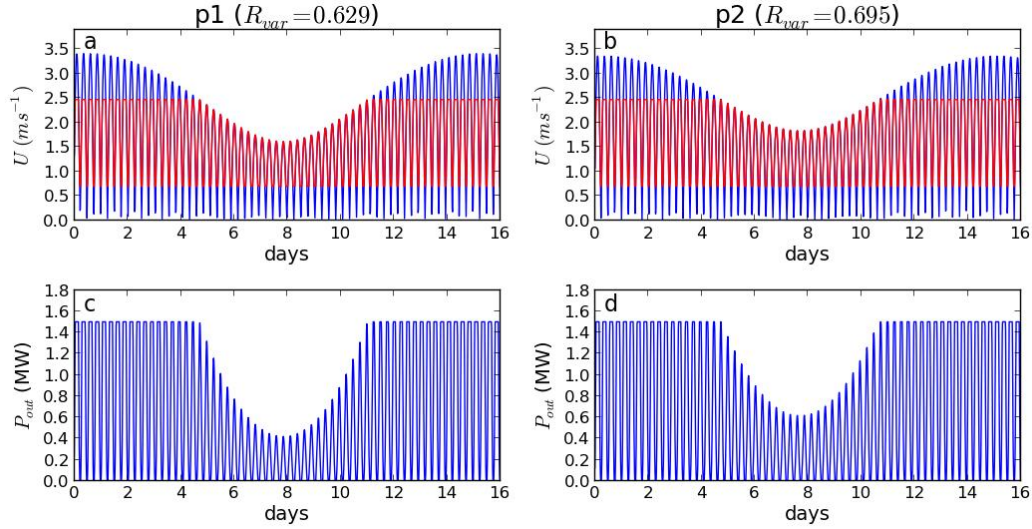


Figure 12: Predicted depth-averaged tidal current velocities  $U$  over a mean spring-neap-spring cycle, and associated generated practical power,  $P_{out}$ , based on the 1.5 MW Open-Hydro power curve in (top) the Fromveur Strait (point p1,  $R_{var} = 0.629$ ) and (bottom) the Alderney Race (point p2,  $R_{var} = 0.695$ ). The red line accounts for the effective tidal velocity which generates power.

390 axis turbines. Indeed, Galloway et al. [40] estimated this limit at  $7.5^\circ$  by  
 391 relying on experimental data and a Blade Element Momentum (BEM) code.  
 392 More recently, Frost et al. [41] demonstrated, from Computational Fluid Dy-  
 393 namics modelling, a drop of 7% in the maximum theoretical available power  
 394 between misalignment angles of  $0$  and  $10^\circ$ . Directional asymmetry exceeds  
 395  $15^\circ$  in limited locations of potential tidal stream energy sites. Confirming the  
 396 investigation conducted by Lewis et al. [26] in the Irish Sea, this concerns  
 397 mainly areas associated with tidal recirculations appearing around Cap de la  
 398 Hague (the north-western headland off the Cotentin Peninsula), and west of  
 399 Alderney and Ushant islands. Taking into account the reduced ellipticity of

400 the current harmonic  $M_2$  in the majority of sites of interest (Section 3.2, Fig.  
401 9), the tidal current appears thus nearly rectilinear during mean spring con-  
402 ditions, an additional condition required to optimise the exploitation of the  
403 tidal kinetic energy resource. Whereas further investigations are required,  
404 relying on refined numerical modelling in potential tidal stream sites and  
405 integrating the influence of a greater number of harmonic components, these  
406 results support the implementation of fixed-orientation (non-yawing) devices.

#### 407 3.4. Asymmetry of tidal currents

408 Fig. 13 shows the spatial distributions of asymmetry metrics  $A_1$  (Eq. 9)  
409 and  $A_2$  (Eq. 10) in western Brittany and the western English Channel. A  
410 close correlation is obtained between both parameters, confirming the relia-  
411 bility of parameter  $A_1$  to characterise the asymmetry of tidal currents from  
412 the amplitude and phase of harmonic components  $M_2$  and  $M_4$ . At regional  
413 scale, numerical results appear consistent with results reported by Robins  
414 et al. [7], exhibiting strong tidal asymmetry in the Channel Island Gulf.  
415 However, the refined spatial resolution in the present study resolves tidal  
416 current asymmetry at the scale of straits, as well as in the vicinity of islands  
417 and headlands. Contrasting asymmetries are thus exhibited between sites.  
418 The region off the Cotentin Peninsula shows globally weak tidal asymmetry,  
419 whereas high values of parameters  $A_1$  and  $A_2$  are obtained in the vicinity of  
420 Alderney and coastal headlands, in relation to the formation of tidal residual  
421 eddies [42].

422 Further, the Fromveur Strait is characterised by pronounced tidal cur-  
423 rent asymmetry. As described elsewhere in the literature [17, 43, 44], this  
424 asymmetry is associated with one area experiencing northeast-directed flood-

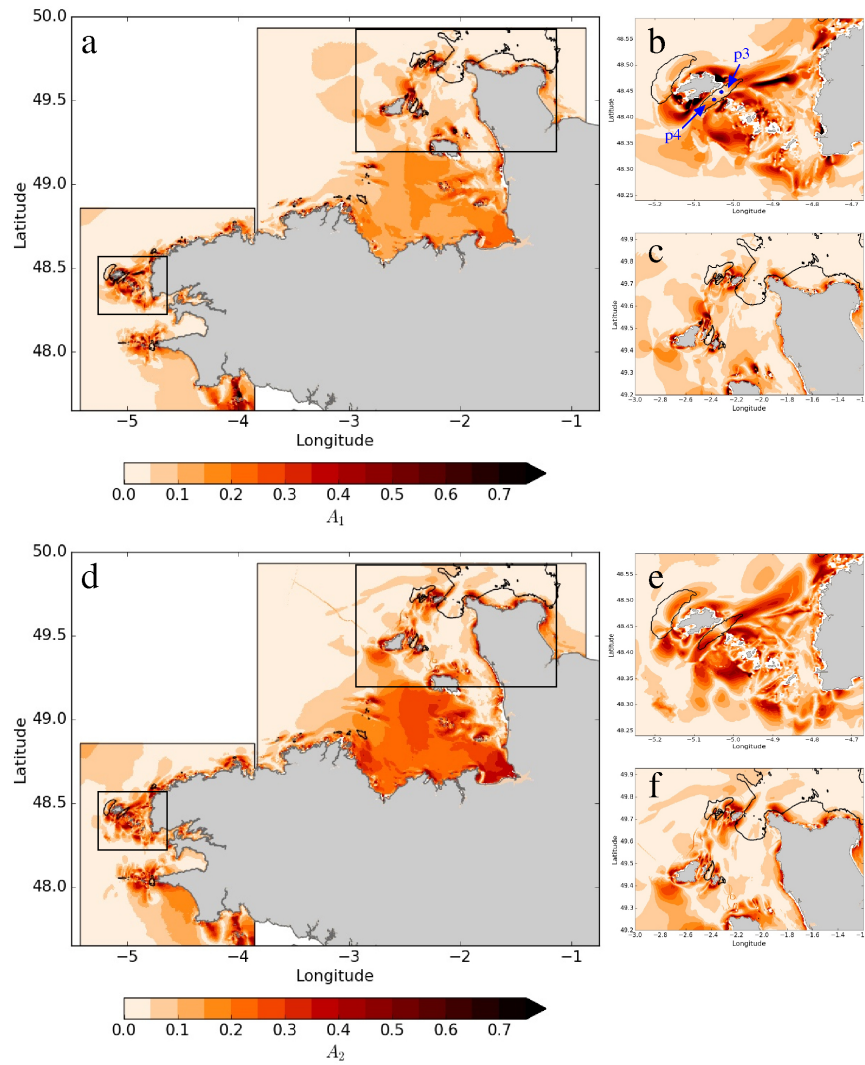


Figure 13: Spatial distribution of parameters  $A_1$  (top) and  $A_2$  (bottom) characterising the asymmetry of tidal currents in (a) coastal domains, with magnified views in (b) the Fromveur Strait and (c) the Alderney Race. The blue circles in (b) show the positions of points p3 and p4 used for the extraction of recomposed currents amplitude and direction in Fig. 14. The black lines delineate potential tidal stream energy sites identified in Fig. 6.

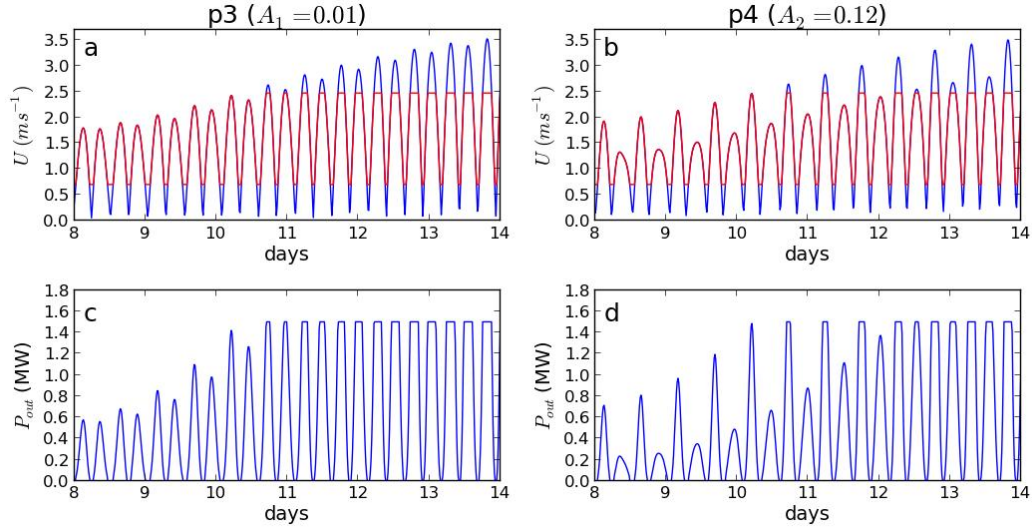


Figure 14: Predicted depth-averaged tidal current speeds  $U$  during mean spring-neap conditions and associated generated practical power,  $P_{out}$ , based on the 1.5 MW OpenHydro power curve in the central (point p3) and southern (point p4) Fromveur Strait. The red line accounts for the effective tidal velocity which generates power.

425 dominated flows, and another area experiencing southward ebb-dominated  
 426 flows. For this region, we confirm the relationship between tidal current  
 427 asymmetry and the relative phase lag of the  $M_2$  component to  $M_4$ , as previ-  
 428 ously shown from surface velocity measurements by Thiébaud and Sentchev  
 429 [43], and from numerical simulations by Guillou and Chapalain [44]. The  
 430 results also confirm the asymmetry in tidal currents off Paimpol-Bréhat re-  
 431 ported by Pham and Martin [45].

432 We extracted depth-averaged tidal velocities from  $M_2$ ,  $S_2$  and  $M_4$  com-  
 433 ponents, and calculated the associated generated practical power from a hy-  
 434 pothetical OpenHydro device at two points in the central (point p3) and  
 435 southern (point p4) Fromveur Strait (Figs. 13-b and 14). The two locations

436 considered are characterised by similar spring-neap tidal variabilities, with  
437 values of parameter  $R_{var} \simeq 0.64$ . At point p3, the flow is largely symmetrical  
438 ( $A_1 = 0.01$ ; Fig. 14-a), with mean spring-neap power estimated at 242 MWh  
439 (Fig. 14-c). However, at point p4, the flow is asymmetrical ( $A_1 = 0.12$ ; Fig.  
440 14-b), with mean spring-neap power estimated as 12% less (213 MWh; Fig.  
441 14-d). During the 6-day period from neap to spring conditions, variations  
442 of peak practical power were up to 1.0 MW between two consecutive tidal  
443 cycles at point p4 (characterised by tidal asymmetry), whereas variations of  
444 p3 were restricted to 0.5 MW. This result suggests that fine scale resource  
445 assessments are beneficial for device optimisation at array scales. Finally, our  
446 results highlight the interest of the Alderney Race, characterised by reduced  
447 tidal current asymmetry (Fig. 13), for the exploitation of the tidal kinetic  
448 energy resource.

#### 449 4. Conclusions

450 A high-resolution tidal harmonic database has been exploited to pro-  
451 vide detailed insights into the characteristics of tidal currents and associated  
452 power in the coastal waters of France, focusing on western Brittany and the  
453 western English Channel – two areas that have strong potential for the ex-  
454 ploitation of the tidal kinetic energy resource. The harmonic database has  
455 been assessed by comparing recomposed tidal water elevations with observa-  
456 tions at a series of harbours along the coasts of France. This evaluation has  
457 been extended by comparing recomposed tidal currents with a series of three  
458 in-situ ADCP datasets available in the vicinity of principal areas identified  
459 for tidal array development. In addition to a map of potential tidal stream



460 energy sites based on current magnitudes and water depths, a method is pro-  
461 posed to exploit, at reduced computational costs, the amplitudes and phases  
462 of current harmonic components, and to characterise the spatial and tempo-  
463 ral variabilities of the resource. The main outcomes of the present study are  
464 as follows:

- 465 1. The resource identified in the western English Channel, off the Cotentin  
466 Peninsula, has great potential for tidal stream energy – comprising  
467 a significant part of the tidal kinetic energy around France. Tidal  
468 currents reach  $4 \text{ m s}^{-1}$  in this region during spring conditions, and the  
469 total exploitable surface area is estimated to be  $1750 \text{ km}^2$ , based on the  
470 criteria of mean spring currents greater than  $2.0 \text{ m s}^{-1}$  and water depths  
471 greater than 25 m. The average power density during mean spring tidal  
472 conditions varies between  $0.9$  and  $12.4 \text{ kW m}^{-2}$ , with a mean value  
473 estimated at  $1.6 \text{ kW m}^{-2}$ . This accounts for a concentration of tidal  
474 stream energy in the Alderney Race, around the Cotentin Peninsula.
- 475 2. Strong values of the kinetic power density (over  $7 \text{ kW m}^{-2}$  during a  
476 mean spring tidal cycle) are also obtained in the western area of Alder-  
477 ney (Casquets) and the Fromveur Strait. Other potential locations in-  
478 clude areas restricted to  $40 \text{ km}^2$ , in the Raz of Sein, off Paimpol-Bréhat,  
479 to the west of Ushant and to the east of Guernsey (Big Roussel).
- 480 3. However, there is significant temporal and spatial variability in the  
481 amplitude and direction of tidal stream power. Such variabilities can  
482 both reduce the total energy yield, and reduce the consistency of the  
483 energy yield over daily-to-fortnightly time scales.
- 484 4. The majority of potential tidal stream energy sites investigated here

485 are characterised by near-rectilinear flows in spring conditions – which  
486 favours the installation of fixed-orientation devices.

487 5. However, some regions show greater spring-neap tidal variability than  
488 others (e.g. less variability to the north-east of the Channel Islands and  
489 more variability in western Brittany). Sites off the Cotentin Peninsula  
490 show, in particular, reduced spring-neap tidal variability, contributing  
491 to reduced variations in energy conversion.

492 6. Tidal currents off the Cotentin Peninsula are largely symmetrical, whereas  
493 more pronounced tidal asymmetry occurs off Paimpol-Bréhat, in the  
494 western part of the Isle of Ushant and in the Fromveur Strait.

495 Our results, established using high-spatial resolutions (250 m), provide po-  
496 tential developers with key information to optimise the design and location of  
497 kinetic energy converters. The series of metrics reported here may help pre-  
498 liminary assessments of resource variability, both spatially and temporally,  
499 particularly useful in areas which have been the subject of a reduced number  
500 of investigations of the tidal stream energy resource. However, such resource  
501 assessment has naturally to be complemented by refined numerical modelling  
502 that integrates, in particular, the complex interactions and modulations of  
503 tidal currents with meteorological forcings (wind, waves), and focusing on  
504 hydrodynamic characteristics throughout the water column.

## 505 **Acknowledgements**

506 The authors are particularly grateful to Lucia Pineau-Guillou (Ifremer)  
507 for providing access to the tidal harmonic database used in the present in-  
508 vestigation (<http://www.marc.ifremer.fr/en/produits>). In-situ observa-

509 tions and bathymetric data used here were provided by the French navy  
510 SHOM (“Service Hydrographique et Océanographique de la Marine”). The  
511 treatment of harmonic components was performed on HPC facilities DATAR-  
512 MOR of “Pôle de Calcul Intensif pour la Mer” (PCIM) ([http://www.ifremer.fr/HYPERLINK\"http://www.ifremer.fr/pcim](http://www.ifremer.fr/HYPERLINK\)). The present paper is a con-  
513 tribution to the research program DIADEME (“Design et InterActions des  
514 Dispositifs d’extraction d’Energie Marine avec l’Environnement”) of the Lab-  
515 oratory of Coastal Engineering and Environment (Cerema, <http://www.cerema.fr>). Simon Neill and Peter Robins acknowledge the support of  
516 the Sêr Cymru National Research Network for Low Carbon, Energy and  
517 the Environment (NRN-LCEE), and also the SEACAMS project, which is  
518 part-funded by the European Unions Convergence European Regional De-  
519 velopment Fund, administered by the Welsh European Funding Office.  
520  
521

## 522 **References**

- 523 [1] D. Magagna, A. Uihlein, Ocean energy development in Europe: Current  
524 status and future perspectives, *International Journal of Marine Energy*  
525 11 (2015) 84–104.
- 526 [2] Black and Veatch, Phase I. UK tidal-stream energy resource assessment,  
527 Tech. rep., London, The Carbon Trust (2004).
- 528 [3] H. Tang, K. Qu, G. Chen, S. Kraatz, N. Aboobaker, C. Jiang, Potential  
529 sites for tidal power generation: A thorough search at coast of New  
530 Jersey, USA, *Renewable and Sustainable Energy Reviews* 39 (2014) 412–  
531 425.

- 532 [4] K. Orhan, R. Mayerle, W. W. Pandoe, Assessment of energy production  
533 potential from tidal stream currents in Indonesia, *Energy Procedia* 76  
534 (2015) 7–16.
- 535 [5] J. Zheng, P. Dai, J. Zhang, Tidal stream energy in China, *Procedia*  
536 *Engineering* 116 (2015) 880–887.
- 537 [6] Z. Defne, K. A. Haas, H. M. Fritz, L. Jiang, S. P. French, X. Shi, B. T.  
538 Smith, V. S. Neary, K. Stewart, National geodatabase of tidal stream  
539 power resource in USA, *Renewable and Sustainable Energy Reviews* 16  
540 (2012) 3326–3338.
- 541 [7] P. Robins, S. Neill, M. Lewis, S. Ward, Characterising the spatial and  
542 temporal variability of the tidal-stream energy resource over the north-  
543 west European shelf seas, *Applied Energy* 147 (2015) 510–522.
- 544 [8] S. Neill, M. Hashemi, M. Lewis, Tidal energy leasing and tidal phasing,  
545 *Renewable Energy* 85 (2016) 580–587.
- 546 [9] S. Neill, M. Hashemi, M. Lewis, The role of tidal asymmetry in char-  
547 acterizing the tidal energy resource of Orkney, *Renewable Energy* 68  
548 (2014) 337–350.
- 549 [10] M. Fornerino, C. L. Provost, A model for prediction of the tidal currents  
550 in the English Channel, *International Hydrographic Review* 2 (1985)  
551 143–166.
- 552 [11] D. T. Pugh, *Tides, Surges and Mean Sea-Level*, John Wiley & Sons,  
553 Natural Environment Research Council, Swindon, UK, 1987.

- 554 [12] M. Piano, S. Neill, M. Lewis, P. Robins, M. Hashemi, A. Davies,  
555 S. Ward, M. Roberts, Tidal stream resource assessment uncertainty due  
556 to flow asymmetry and turbine yaw misalignment, *Renewable Energy*  
557 114 (2017) 1363–1375.
- 558 [13] G. Egbert, S. Y. Erofeeva, Efficient Inverse Modeling of Barotropic  
559 Ocean Tides, *Journal of Atmospheric and Oceanic Technology* 19 (2002)  
560 183–204.
- 561 [14] A. Bahaj, L. Myers, Analytical estimates of the energy yield potential  
562 from the Alderney Race (Channel Islands) using maring current energy  
563 converters, *Renewable Energy* 29 (2004) 1931–1945.
- 564 [15] J. Thiébot, P. Bailly du Bois, S. Guillou, Numerical modeling of the  
565 effect of tidal stream turbines on the hydrodynamics and the sediment  
566 transport - Application to the Alderney Race (Raz Blanchard), France,  
567 *Renewable Energy* 75 (2015) 356–365.
- 568 [16] N. Guillou, G. Chapalain, S. P. Neill, The influence of waves on the tidal  
569 kinetic energy resource at a tidal stream energy site, *Applied Energy* 180  
570 (2016) 402–415.
- 571 [17] N. Guillou, J. Thiébot, The impact of seabed rock roughness on tidal  
572 stream power extraction, *Energy* 112 (2016) 762–773.
- 573 [18] D. S. Coles, L. S. Blunden, A. S. Bahaj, Assessment of the energy ex-  
574 traction potential at tidal sites around the Channel Islands, *Energy* 124  
575 (2017) 171–186.

- 576 [19] P. Lazure, F. Dumas, An external-internal mode coupling for a 3D hy-  
577 drodynamical model for applications at regional scale (MARS)., Ad-  
578 vances in Water Resources 31 (2008) 233–250.
- 579 [20] L. Pineau-Guillou, PREVIMER Validation des atlas de composantes  
580 harmoniques de hauteurs et courants de marée, Technical Report  
581 ODE/DYNECO/PHYSED/2013-03 version 1.0, Ifremer (2013).
- 582 [21] R. Le Roy, B. Simon, Réalisation et validation d’un modèle de marée  
583 en Manche et dans le Golfe de Gascogne. Application à la réalisation  
584 d’un nouveau programme de réduction des sondages bathymétriques,  
585 Technical Report 002/03, Service Hydrographique et Océanographique  
586 de la Marine (2003).
- 587 [22] P. Courtier, J. Thepaut, A. Hollingsworth, A strategy for operational  
588 implementation of 4D-VAR, using incremental approach, Quaterly Jour-  
589 nal of the Royal Meteorological Society 120 (1994) 1367–1387.
- 590 [23] Y. Seity, P. Brousseau, S. Malardel, G. Hello, P. Bénard, F. Bouttier,  
591 C. Lac, V. Masson, The AROME-France convective scale operational  
592 model, Monthly Weather Review 139 (2011) 976–991.
- 593 [24] D. Allain, TUGOm Tidal Toolbox, Documentation available at  
594 *ftp://ftp.legos.obs-mip.fr/pub/ecola/tools/ttb.pdf* (2016).
- 595 [25] R. Bedard, M. Previsic, O. Siddiqui, G. Hagerman, M. Robinson, Survey  
596 and Characterization of Tidal In Stream Energy Conversion (TISEC)  
597 Devices, Tech. rep., EPRI (2005).

- 598 [26] M. Lewis, S. Neill, P. Robins, M. Hashemi, Resource assessment for  
599 future generations of tidal-stream energy arrays, *Energy* 83 (2015) 403–  
600 415.
- 601 [27] R. D. Pingree, D. K. Griffiths, Sand transport paths around the British  
602 Isles resulting from  $M_2$  and  $M_4$  tidal interactions, *Journal of the Marine*  
603 *Biological Association of the United Kingdom* 59 (1979) 497–513.
- 604 [28] C. T. Friedrichs, D. G. Aubrey, Non-linear tidal distortion in shallow  
605 well-mixed estuaries: a synthesis, *Estuarine, Coastal and Shelf Science*  
606 27 (1988) 521–545.
- 607 [29] L. Pineau-Guillou, PREVIMER Validation des modèles hydrody-  
608 namiques 2D des côtes de la Manche et de l’Atlantique, Technical Report  
609 ODE/DYNECO/PHYSED/2013-05 version 1.0, Ifremer (2013).
- 610 [30] P. Bailly du Bois, F. Dumas, L. Solier, C. Voiseux, In-situ database  
611 toolbox for short-term dispersion model validation in macro-tidal seas,  
612 application for 2D-model, *Continental Shelf Research* 36 (2012) 63–82.
- 613 [31] C. J. Willmott, On the validation of models, *Physical Geography* 2 (2)  
614 (1981) 219–232.
- 615 [32] SHOM, Courants de marée - Mer d’Iroise de l’île Vierge à la pointe  
616 de Penmarc’h, Technical Report 560-UJA, Service Hydrographique et  
617 Océanographique de la Marine (2016).
- 618 [33] Black and Veatch, Phase II. UK tidal-stream energy resource assess-  
619 ment, Tech. rep., London, The Carbon Trust (2005).

- 620 [34] A. S. Iyer, S. J. Couch, G. P. Harrison, A. R. Wallace, Variability and  
621 phasing of tidal current energy around the United Kingdom, *Renewable*  
622 *Energy* 51 (2013) 343–357.
- 623 [35] L. Biscara, A. Maspataud, T. Schmitt, Présentation de la gamme de  
624 MNT bathymétriques pour la modélisation océanographique (projets  
625 HOMONIM et TANDEM), in: *Colloque merIGéo*, 2015.
- 626 [36] SHOM, MNT Bathymétrie de la façade Atlan-  
627 tique (Projet HOMONIM), Documentation available at  
628 *diffusion.shom.fr/produits/bathymetrie/mnt-facade-atl-homonim.html*  
629 (2017).
- 630 [37] Black and Veatch, UK tidal current resource and economics, Tech. rep.,  
631 Commissioned by the Carbon Trust and npower, Project number 121393  
632 (2011).
- 633 [38] Environmental Change Institute, Variability in UK marine resources,  
634 Technical Report, Commissioned by the Carbon Trust (2005).
- 635 [39] C. Christian, R. Vennel, Efficiency of tidal turbine farms, in: *Coastal*  
636 *Engineering* 2012.
- 637 [40] P. Galloway, L. Myers, A. Bahaj, Experimental and numerical results  
638 of rotor power and thrust of a tidal turbine operating at yaw and in  
639 waves, in: *World Renewable Energy Congress 2011 - Marine and Ocean*  
640 *Technology*, Linköping, Sweden, 2011.
- 641 [41] C. Frost, P. Evans, M. H. an A. Mason-Jones, T. O’Doherty,



- 642 D. O'Doherty, The impact of axial flow misalignment on a tidal tur-  
643 bine, *Renewable Energy* 113 (2017) 1333–1344.
- 644 [42] S. Neill, J. Jordan, S. Couch, Impact of tidal energy convertor (TEC)  
645 arrays on the dynamics of headland sand banks, *Renewable Energy* 37  
646 (2012) 387–397.
- 647 [43] M. Thiébaud, A. Sentchev, Asymmetry of tidal currents off the Western  
648 Brittany coast and assessment of tidal energy resource around Ushant  
649 Island, *Renewable Energy* 105 (2017) 735–747.
- 650 [44] N. Guillou, G. Chapalain, Assessing the impact of tidal stream energy  
651 extraction on the Lagrangian circulation, *Applied Energy* 203 (2017)  
652 321–332.
- 653 [45] C. Pham, V. Martin, Tidal current turbine demonstration farm in  
654 Paimpol-Bréhat (Brittany): tidal characterisation and energy yield eval-  
655 uation with Telemac, in: *Proceedings of the 8th European Wave and*  
656 *Tidal Energy Conference*, Uppsala, Sweden, 2009.